Supplementary Material for: Fast recovery of the stripe magnetic order by Mn/Fe substitution in F-doped LaFeAsO superconductors

M. Moroni,[1,*] P. Carretta,[1] G. Allodi,[2] R. De Renzi,[2] M. N. Gastiasoro,[3] B. M. Andersen,[3] P. Materne,[4] H.-H. Klauss,[4] Y. Kobayashi,[5] M. Sato,[5] and S. Sanna[1,6]

[1] *Department of Physics, University of Pavia-CNISM, I-27100 Pavia, Italy*
[2] *Dipartimento di Fisica e Scienze della Terra, Università di Parma, I-43124 Parma, Italy*
[3] *Niels Bohr Institute, University of Copenhagen, Juliane Maries Vej 30, 2100 Copenhagen, Denmark*
[4] *Institute of Solid State Physics, TU Dresden, D-01069 Dresden, Germany*
[5] *Department of Physics, Division of Material Sciences, Nagoya University, Furo-cho, Chikusa-ku, Nagoya 464-8602, Japan*
[6] *Department of Physics and Astronomy, University of Bologna, 40127 Bologna, Italy*

I. SAMPLE PREPARATION AND CHARACTERIZATION.

In the present study we have presented data for two series of samples (say, #A and #B) among many series showing a very similar trend of T_c with Mn doping. The samples with the Mn concentration x = 0.5% and 0.75% belong to #A, and x=0.075% and 0.2% belong to #B. The x=0 sample displays an almost optimum value of T_c=27 K by SQUID magnetometry and muon spin rotation measurements, as reported in Ref.[1]. Despite this fact, Fig. 4a shows that its high temperature NQR spectrum is characterized by a double peak structure, typically observed in the underdoped compounds [2, 3] where charge-poor and charge-rich environments coexist at the nanoscale. Hence, following Ref. [2], the NQR results show that the whole set of samples displays intrinsic electronic inhomogeneity, as pointed out for x=0-0.2 in Ref.[1]. The intensity of the ^{19}F NMR signal measured at room temperature shows that the fluorine content is constant throughout all the samples within an accuracy of $\Delta y = 2\%$.

II. MÖSSBAUER MEASUREMENTS

The Mössbauer measurements were performed in transmission geometry in the 2.3 K - 300 K temperature range using a CryoVac Konti IT cryostat on the $LaFe_{1-x}Mn_xAsO_{0.89}F_{0.11}$ for x=0.5%. As the γ source, a ^{57}Co in rhodium matrix was used. We used Ferrocen powder to measure the influence of the experiment on the line width. The data was analyzed using the transmission integral. Mössbauer data for representative temperatures above and below T_m are shown in Fig. 1. At all investigated temperatures a three peak structure is observed. The two outer peaks at $\approx$ - 0.80 and 1.65 mm/s correspond to the Ferrocen reference absorber while the inner peak is identified with the $LaFe_{1-x}Mn_xAsO_{0.89}F_{0.11}$. At 296 K a non-resolved doublet structure is observed due to the interaction of the nucleus with an electric field gradient (EFG). In the principal-axis system, the EFG is fully determined by its z component V_{ZZ} and the asymmetry parameter $\eta = (V_{XX} - V_{YY})/V_{ZZ}$. We obtained a center shift of 0.451(1) mm/s and a value of $V_{ZZ} = 4.5$ V/Å^2. η was found to be zero at all temperatures. The center shift increases upon cooling due to the temperature-dependent second-order Doppler effect to a value of 0.586(8) mm/s at 4.2 K. V_{ZZ} increases with decreasing temperature to a value of 8.6 V/Å^2 at 82 K. At the magnetic phase transition V_{ZZ} increases to 12(2) V/Å^2 and remains constant within error bars down to lowest temperatures. This change of the the electric field gradient probed by Fe around the magnetic transition reflects the structural T-O transition in agreement with the one probed by As in the NQR measurements discussed in the main text. Below T_m a broad peak is observed which is identified with a non-resolved sextet structure due to a field distribution. This magnetic field distribution was modeled using a Gaussian distribution. The temperature dependence of the first moment is shown in Fig. 1c of the main part of the paper.

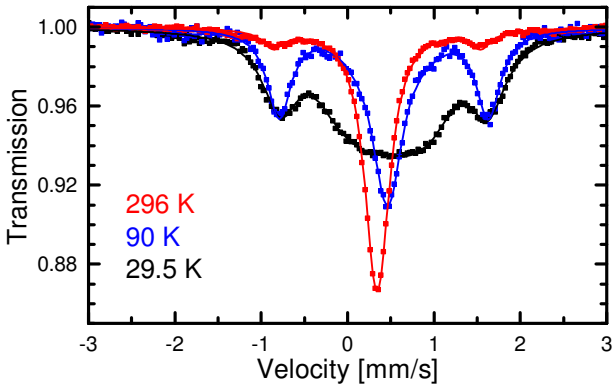

FIG. 1. Mössbauer spectra for the $x = 0.5\%$ compound at a few selected temperatures both above and below T_m.

III. NQR AND NMR SPECTRA

In order to carry out the NMR experiments the polycrystalline $LaFe_{1-x}Mn_xAsO_{0.89}F_{0.11}$ samples were crushed to a fine powder to improve radio frequency penetration. Since ^{75}As is a spin I = 3/2 nucleus, above T_m, the NQR spectrum is characterized by a single line at a frequency

$$\nu_Q = \frac{eQV_{ZZ}}{2h}\left(1+\frac{\eta^2}{3}\right)^{1/2} \quad (1)$$

with Q the electric quadrupole moment of the ^{75}As nucleus, V_{ZZ} the main component of the electric field gradient (EFG) tensor at the As site generated by the surrounding charge distribution and η its asymmetry. Since LaFeAsO is tetragonal $\eta = 0$ and c is the quantization axis. Thus, the broadening of the line is mainly due to the disorder present in the system since the EFG strongly depends on the local charge distribution. The two peak in the NQR spectra (Fig.4, main article) are due to an intrinsic electronic inhomogeneity (due to F doping) already present without Mn in superconducting samples where the whole volume is superconducting (see Ref. 2).

Below T_m, in case of a stripe magnetic order, an internal field $H_{int} \parallel c$ is present at the As nuclei and we can perform standard NMR experiments with the only difference that the magnetic field is not provided by an external magnet but by the magnetic ordering of the Fe moments (see also the main part of the paper). Even if below T_m the unit cell is orthorhombic the asymmetry η is still small ($\eta \sim 0.15$) as reported in Ref. [4].

^{75}As NQR and ZF-NMR spectra were derived by recording the integral of the echo signal after a $\pi/2-\tau_e-\pi$ pulse sequence as a function of the irradiation frequency. All the ZF-NMR spectra were measured with exactly the same set-up and coil filling factor in order to compare the relative intensity of the lines. It must also be noted that the length of the pulses was optimized for the $m_I = -1/2 \rightarrow m_I = -3/2$ line and kept constant for the whole spectrum. However the resulting distortion in the spectrum amplitude is not sample dependent and does not modify the position of the lines.

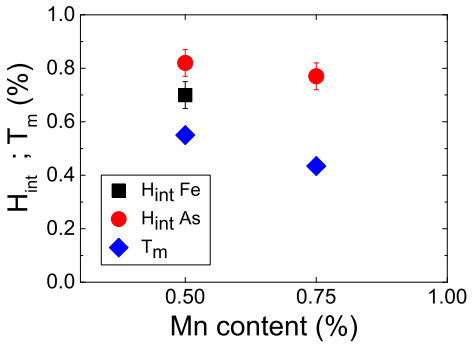

FIG. 2. Intensities of the hyperfine magnetic fields at the As (H_{int} As) and Fe (H_{int} Fe) sites at 8 K in $LaFe_{1-x}Mn_xAsO_{0.89}F_{0.11}$ (x =0.5 % and x =0.75 %) normalized to those measured in undoped LaFeAsO. The hyperfine fields at the two sites were measured respectively with ZF-NMR and Mössbauer spectroscopy. The relative magnetic transition temperature, measured with ZF-μSR, is also reported. The reference values measured in LaFeAso are: T_m = 145 K, H_{int} As = 1.6 T and H_{int} Fe = 5 T.

The resulting spectra both for undoped LaFeAsO and for $LaFe_{1-x}Mn_xAsO_{0.89}F_{0.11}$ samples are reported in Fig. 1a of the main part of the paper. Since, the stripe magnetic order is also present in $LaFe_{1-x}Mn_xAsO_{0.89}F_{0.11}$ (see next section) we can derive the intensity of the hyperfine field at the As site from the frequency $\nu_c = (\gamma/2\pi)|\mathcal{A}\langle\vec{S}\rangle| = (\gamma/2\pi)H_{int}$ of the low-frequency line corresponding to the $m_I = 1/2 \rightarrow m_I = -1/2$ transition (see main part). The results are reported in Fig. 2.

The ^{75}As NMR experiments were performed by a homemade NMR spectrometer and a home-assembled probehead placed in the variable-temperature insert of a field-sweeping cold-bore cryomagnet. The large capacitance span of the variable capacitor in the probehead (approx. 2-100 pF) provides a tuning range of more than two octaves. This allowed us to cover the entire spectral range of the ^{75}As and ^{139}La resonances at 8 T with a single coil. The usage of the same coil for all the resonances, along with a careful calibration of the frequency response of the spectrometer, ensures a reliable quantitative comparison of the amplitudes from different spectral features.

The spectra were recorded by tuning the probehead at discrete frequency steps by means of a software-controlled servomechanism featured by the spectrometer itself, and exciting a spin echo. The spin-echo sequence was a standard $P-\tau-P$ one, with equal rf pulses P of duration $\approx 12-16\ \mu s$ and intensity suitably adjusted to optimize the signal. The delays τ was kept as short as possible with respect to the dead time of the resonant probehead (≈20-35μs depending on the working frequency).

The fraction of nuclei participating in the majority and minority ^{75}As signals, respectively, was estimated from the integral of the the normalized spectral amplitude (i.e. the amplitude divided by the frequency dependent sensitivity $\propto \omega^2$). In the case of the minority signal, characterized by a hyperfine field estimated in the order of 8-10 T from the NMR spectra in lower external fields (not shown), a further correction factor is given by the rf enhancement α originating from the hyperfine coupling between electronic and nuclear spins. Such a coupling, on one hand, amplifies the driving rf field at the nucleus, so that the resonance can be excited by a rf field reduced by α; on the other, it enhances the e.m.f. induced in the pick-up by the same factor. In a strong external field B_{ext} as in the present case, a factor of the order of

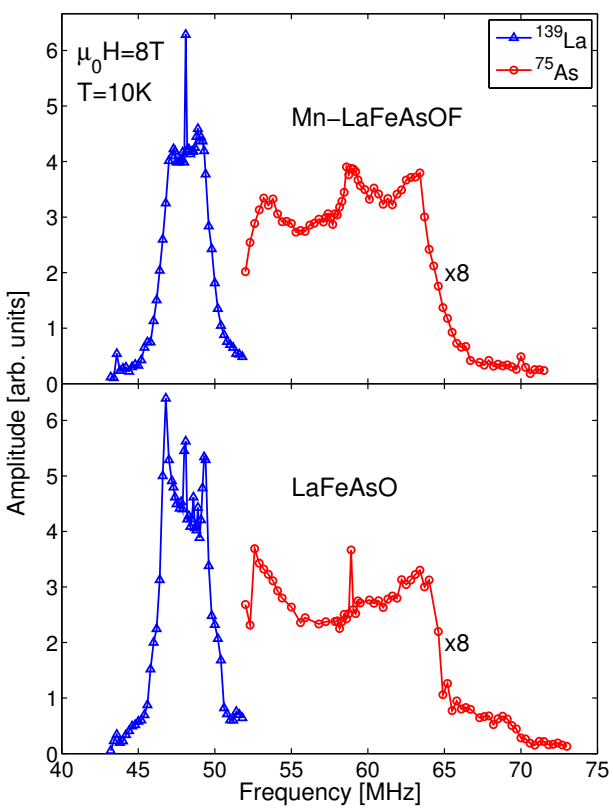

FIG. 3. Top: ^{75}As (majority signal) and ^{139}La NMR spectra of $LaFe_{1-x}Mn_xAsO_{0.89}F_{0.11}$ x=0.5% at $T = 10$ K and $\mu_0 H_0 = 8$ T. Bottom: ^{75}As and ^{139}La spectra of the parent compound, LaFeAsO, at the same temperature and applied field

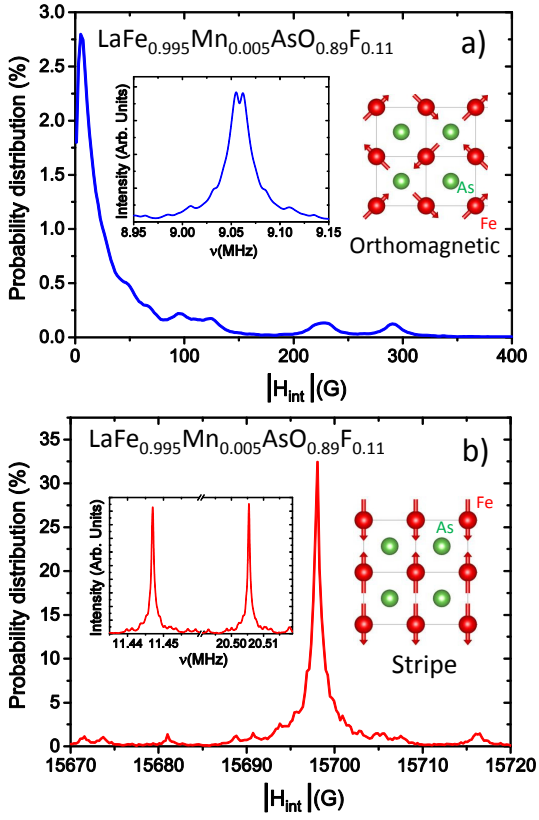

FIG. 4. Simulated (see text) distribution of internal fields on the As site (main panels) and simulated ^{75}As ZF-NMR spectra (left insets) of $LaFe_{0.995}Mn_{0.005}AsO_{0.89}F_{0.11}$ in case of orthomagnetic order (a) and stripe order (b). In this simulation Mn impurities takes part to the magnetic ordering so their moments have the same orientation of the magnetic moment of the substituted Fe ion, pictorially shown in the right insets.

$\alpha \approx B_{eff}/B_{ext}$ (a formula strictly valid for a uniaxial ferromagnet, indeed), where B_{eff} is the effective field at the nucleus, is expected, [5] hence $\alpha \leq 2$. A similar value of $\alpha \approx 2$ is obtained by comparing the excitation conditions for the two signals, as the minority signal was optimally excited with 6dB extra-attenuation. After correcting (i.e. dividing) the minority signal amplitude by $\alpha = 2$, we obtained our estimate for the volume fraction of the minority estimate ^{75}As nuclei in the order of 3% of total. Figure 3 shows that the As spectrum of the magnetic ordered state in x=0.5% Mn doped $LaFeAsO_{0.89}F_{0.11}$, appearing also in Fig. 2 (main part), is extremely similar to that of the parent compound LaFeAsO, without F doping. This observation provides further evidence that the magnetic orders present in the two compounds is indeed the same.

IV. INTERNAL FIELD CALCULATIONS

In order to interpret the ZF-NMR results we performed simulations of the internal field at the As site for different types of long range magnetic order and for various Mn concentrations. Both the long range dipolar interaction and the short range transferred hyperfine interaction between the As nucleus and magnetic moments on the four nearest neighbor Fe ions (see Fig. 1) have been considered in the calculations. The internal field can be written as the sum of the contributions from each one of the Fe sites:

$$\mathbf{H}_{\rm int} = \sum_i \mathbf{A}_i \cdot \mathbf{m}_i \qquad (2)$$

where $\mathbf{m}_i$ is the ordered electron moment at the i-th Fe site and $\mathbf{A}_i$ is the nuclear-electron coupling tensor between the As nucleus and i-th Fe site. We considered only the contributions due to the Fe sites in the same plane of the As nucleus since the contribution to the internal field from the other Fe-As layers is vanishingly small due to the r^{-3} scaling of the dipolar coupling. The diagonal components of the symmetric transferred hyperfine interaction tensor for the four nearest neighbor Fe sites (Fig. 5) was derived from Knight shift measurements while two of the three off diagonal components can be derived from the strength of the internal field in the stripe order configu-

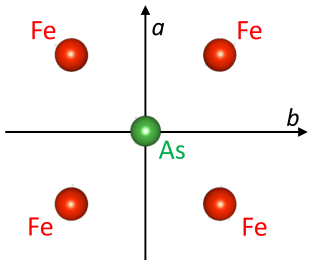

FIG. 5. Sketch of the nearest neighbor Fe sites around an As nucleus in the orthorhombic unit cell. The As does not lie on the same plane of the four Fe sites.

ration, as reported in Ref. 7. Since we are only interested in understanding which types of order give rise to spectra in qualitative agreement with the measured ones, we used the values of the transferred hyperfine tensor components reported in Ref. 6 and chose $m_{Fe} = 0.36\ \mu_B$ for the Fe magnetic moment and $m_{Mn} = 4\ \mu_B$ for the Mn magnetic moment. The third off-diagonal component of the transferred hyperfine coupling is relevant only in case of Neel order and was chosen equal to the stripe one. The distribution of the internal fields for each type of magnetic order was calculated by randomly substituting Mn (for $x = 0.5$ %) on the Fe site in a 24×24 size mesh and repeating the calculation 10^5 times. The spectra were then obtained by diagonalizing the Zeeman-Quadrupole Hamiltonian:

$$\mathcal{H} = \mathcal{H}_{\rm Zeeman} + \mathcal{H}_Q = \tag{3}$$
$$= -\gamma\hbar\mathbf{H}_{\rm int}\cdot\mathbf{I} + \frac{eQV_{ZZ}}{12}[3\mathrm{I}_z^2 - \mathrm{I}^2 + \eta(\mathrm{I}_x^2 - \mathrm{I}_y^2)]$$

for each value of the magnetic field and applying magnetic dipole selection rules. The results for orthomagnetic and stripe order are reported in Fig. 4. For the orthomagnetic order we found $\mathrm{H_{int}} \sim 0$. This value is incompatible with the resonance frequency measured by ^{75} ZF-NMR for x=0.5 % and 0.75 % (main part Fig. 1a), which displays a sizable internal field with about 80 % of the value found for pure LaFeAsO. In case of Néel order the internal field is found to be $\mathrm{H_{int}} > 1$ T. However in this magnetic structure the field is parallel to a and the splitting between the NQR lines is expected to be half of the observed one. Another possible type of magnetic structure is the spin-charge order [8] which should give rise to two inequivalent iron sites. But this is in contrast with the Mössbauer measurements which reveal only one iron site. Therefore, the only magnetic structure compatible with the observed experimental results is the (π,0) or (0,π) stripe ordering. In addition, one must notice that the linewidth induced by the magnetic disorder is three orders of magnitude smaller than the one measured. This prediction is in good agreement with the observation that no significant change is induced in the line width by increasing the Mn content from 0.5 % to 0.75%. Conversely as can be seen in the NQR spectra (see Ref. [2]) fluorine doping has a strong effect on the line width. This implies that the line broadening of $\mathrm{LaFe_{1-x}Mn_xAsO_{0.89}F_{0.11}}$ (x=0.5 % and 0.75 %) with respect to LaFeAsO is mostly due to the disorder induced by F doping and possibly by the magnetic disorder related to the formation of (0,π) and (π,0) magnetic domains that get pinned by the Mn impurities (see Fig. 5 in the main part). Finally it must be noted that we cannot completely rule out the presence of an incommensurate magnetic order with magnetic wave vector very close to the stripe one. In fact the incommensurability leads to a broadening of the ZF-NMR line, which, in this case, would be impossible to observe since it can be much smaller than the line broadening due to fluorine doping.

V. MODEL

A proper modelling of $\mathrm{LaFe_{1-x}Mn_xAsO_{0.89}F_{0.11}}$ includes both a realistic (five-orbital) model of the kinetic energy

$$\mathcal{H}_0 = \sum_{\mathbf{ij},\mu\nu,\sigma} t_{\mathbf{ij}}^{\mu\nu}\hat{c}_{\mathbf{i}\mu\sigma}^\dagger\hat{c}_{\mathbf{j}\nu\sigma} - \mu_0\sum_{\mathbf{i}\mu\sigma}\hat{n}_{\mathbf{i}\mu\sigma}, \tag{4}$$

with tight-binding parameters determined in Ref. 9, and inclusion of electronic interactions given by the multi-orbital Hubbard Hamiltonian

$$\mathcal{H}_{int} = U\sum_{\mathbf{i},\mu}\hat{n}_{\mathbf{i}\mu\uparrow}\hat{n}_{\mathbf{i}\mu\downarrow} + (U' - \frac{J}{2})\sum_{\mathbf{i},\mu<\nu,\sigma\sigma'}\hat{n}_{\mathbf{i}\mu\sigma}\hat{n}_{\mathbf{i}\nu\sigma'} \tag{5}$$
$$- 2J\sum_{\mathbf{i},\mu<\nu}\vec{S}_{\mathbf{i}\mu}\cdot\vec{S}_{\mathbf{i}\nu} + J'\sum_{\mathbf{i},\mu<\nu,\sigma}\hat{c}_{\mathbf{i}\mu\sigma}^\dagger\hat{c}_{\mathbf{i}\mu\bar{\sigma}}^\dagger\hat{c}_{\mathbf{i}\nu\bar{\sigma}}\hat{c}_{\mathbf{i}\nu\sigma},$$

Here μ, ν are orbital indexes, $\mathbf{i}$ denotes lattice sites, and σ is the spin. The interaction includes intraorbital (interorbital) repulsion U (U'), the Hund's coupling J, and the pair hopping energy J'. We assume $U' = U - 2J$, $J' = J$, and choose $J = U/4$. Superconductivity is included by a BCS-like term

$$\mathcal{H}_{BCS} = -\sum_{\mathbf{i}\neq\mathbf{j},\mu\nu}[\Delta_{\mathbf{ij}}^{\mu\nu}\hat{c}_{\mathbf{i}\mu\uparrow}^\dagger\hat{c}_{\mathbf{j}\nu\downarrow}^\dagger + \mathrm{H.c.}], \tag{6}$$

with $\Delta_{\mathbf{ij}}^{\mu\nu} = \sum_{\alpha\beta}\Gamma_{\mu\alpha}^{\beta\nu}(\mathbf{r_{ij}})\langle\hat{c}_{\mathbf{j}\beta\downarrow}\hat{c}_{\mathbf{i}\alpha\uparrow}\rangle$ being the superconducting order parameter, and $\Gamma_{\mu\alpha}^{\beta\nu}(\mathbf{r_{ij}})$ denoting the effective pairing strength between sites (orbitals) $\mathbf{i}$ and $\mathbf{j}$ (μ, ν, α and β). In agreement with a general $s^\pm$ pairing state, we include next-nearest neighbor (NNN) intra-orbital pairing, $\Gamma_\mu \equiv \Gamma_{\mu\mu}^{\mu\mu}(\mathbf{r_{nnn}})$. Magnetic disorder modeling the Mn moments is included by $\mathcal{H}_{imp} = I\sum_{\{\mathbf{i}^*\}\mu\sigma}\sigma S_\mu c_{\mathbf{i}^*\mu\sigma}^\dagger c_{\mathbf{i}^*\mu\sigma}$, where S_μ is magnetic moment in orbital μ at the disorder sites given by the set $\{\mathbf{i}^*\}$ coupled to the spin density of the itinerant electrons.

After a mean-field decoupling of the interacting Hamiltonian we solve the Bogoliubov-de Gennes equations,

$$\begin{pmatrix} \hat{\xi}_{\uparrow} & \hat{\Delta}_{\mathbf{ij}} \\ \hat{\Delta}^{*}_{\mathbf{ji}} & -\hat{\xi}^{*}_{\downarrow} \end{pmatrix} \begin{pmatrix} u^n \\ v^n \end{pmatrix} = E_n \begin{pmatrix} u^n \\ v^n \end{pmatrix}, \tag{7}$$

where

$$\begin{aligned} \hat{\xi}_{\sigma} u_{\mathbf{i}\mu} = & \sum_{j\nu} t^{\mu\nu}_{\mathbf{ij}} u_{\mathbf{j}\nu} + \sum_{\mu\neq\nu} [-\mu_0 + \sigma I S_{\mu} \delta_{\mathbf{i}\{\mathbf{i}^*\}} \delta_{\mu\nu} U n_{\mathbf{i}\mu\bar{\sigma}} \\ & + U' n_{\mathbf{i}\nu\bar{\sigma}} + (U' - J) n_{\mathbf{i}\nu\sigma}] u_{\mathbf{i}\mu} \ , \end{aligned} \tag{8}$$

$$\hat{\Delta}^{\mu\nu}_{\mathbf{ij}} u_{\mathbf{i}\mu} = -\sum_{\mathbf{j}\nu} \Delta^{\mu\nu}_{\mathbf{ij}} u_{\mathbf{j}\nu}.$$

The five-orbital BdG equations are solved on 30×30 lattices with stable solutions found through iterations of the following self-consistency equations

$$\begin{aligned} n_{\mathbf{i}\mu\uparrow} &= \sum_n |u^n_{\mathbf{i}\mu}|^2 f(E_n), \\ n_{\mathbf{i}\mu\downarrow} &= \sum_n |v^n_{\mathbf{i}\mu}|^2 (1 - f(E_n)), \\ \Delta^{\mu}_{\mathbf{ij}} &= \Gamma_{\mu} \sum_n u^n_{\mathbf{i}\mu} v^{n*}_{\mathbf{j}\nu} f(E_n), \end{aligned} \tag{9}$$

where $\sum_n$ denotes summation over all eigenstates n and $f(E)$ denotes the Fermi function. We stress that the solutions are fully unrestricted and allowed to vary on all lattice sites and orbitals. Finally the relative signs of the individual impurity spins σS_{μ} are obtained by minimizing the total free energy of the system. We operate in the regime of interactions where the impurity-free system is paramagnetic ($U < 0.9$ eV). For the results in Fig. 5, we have used $U = 0.87$eV, $kT = 0.001$eV, $IS_{\mu} = 0.38$eV. A comprehensive description of the band structure and all details of the self-consistent solutions of the mean-field decoupled Hamiltonian in real-space can be found in Ref. 10 and its associated Supp. Material.

Finally we would like to remark that the results clearly show that there is a critical concentration of Mn above which the system leaves the SC phase and is back to the stripe phase which also characterize the undoped LaFeAsO. The critical concentration inferred from the calculation is in good agreement with the experimental one. While the mean distance between Mn impurities is clearly an essential parameter it should be remarked that the recovery of magnetism is a collective and non-local effect so the number of Mn ions is a particular region of the system (e.g. magnetic domains) is not so important (see Fig. 5, main article). For small Mn concentrations no FM/AFM alternation is predicted and anyway such a property is usually not observed in disordered alloys.

* matteo.moroni01@universitadipavia.it

[1] F. Hammerath, P. Bonfá, S. Sanna, G. Prando, R. De Renzi, Y. Kobayashi, M. Sato, and P. Carretta, Phys. Rev. B **89**, 134503 (2014).

[2] G. Lang et al., Phys. Rev. Lett. **104**, 097001 (2010).

[3] Y. Kobayashi, E. Satomi, S. C. Lee, M. Sato, J. Phys. Soc. Japan **79**, 093709 (2010).

[4] M.Fu et al., Phys. Rev. Lett. **109**, 247001 (2012).

[5] P. C. Riedi, Hyperfine Interact. **49**, 335 (1989)

[6] S. Kitagawa, Y. Nakai, T. Iye, K. Ishida, Y. Kamihara, M. Hirano, H. Hosono, Phys. Rev. B, **81**, 212502 (2010).

[7] K. Kitagawa, N. Katayama, K. Ohgushi, M. Yoshida, M. Takigawa, J. Phys. Soc. Jpn. **77**, 114709 (2008).

[8] G. Giovannetti, C. Ortix, M. Marsman, M. Capone, J. van den Brink, and J. Lorenzana, Nat. Commun. **2**, 398 (2011).

[9] H. Ikeda, R. Arita, and J. Kunes, Phys. Rev. B **81**, 054502 (2010).

[10] M. N. Gastiasoro, F. Bernardini, B. M. Andersen, Phys. Rev. Lett. **117**, 257002 (2016).